Sparse Recovery Transmitter Detection

Blessing Okoro, Maxwell McNeil, Kavya Meka, Karyn Doke, Petko Bogdanov, Mariya Zheleva
Department of Computer Science, University at Albany, SUNY, USA.
{aaokoro, mmcneil2, kmeka2, kdoke, pbogdanov, mzheleva}@albany.edu

***Abstract*—Transmitter detection and separation in radio spectrum scans is an essential component in emerging spectrum-sharing networks, as it underpins situational awareness for coexistence and enforcement. However, detecting transmitters in noisy real-world traces is challenging and has been tackled with limited practical applicability. Beyond noisy measurements, the challenges stem from the need to simultaneously detect multiple and possibly overlapping transmitter frequency bands and track their transmissions over time.**

We address these challenges with SCAN (Sparse reCovery trAnsmitter detectioN): an unsupervised approach based on sparse dictionary coding to jointly detect the frequency and temporal behavior of multiple co-occurring transmitters in power spectral density traces. We demonstrate SCAN's applicability to high-noise regimes and across various transmitter co-occurrence scenarios, including when transmitters concurrently overlap in time and frequency (akin to intentional or unintentional interference). We evaluated SCAN's performance with synthetic and real-world traces and in comparison with baselines. We show that SCAN can characterize multiple transmitters even when their power levels are the same. Furthermore, SCAN successfully detects and characterizes 10 simultaneously observed transmitters, whereas counterparts fall short even in 3-transmitter scenarios. Finally, we demonstrate that SCAN can discern real-world activity with WiFi, ZigBee, LTE and LoRa transmitters.

***Index Terms*—spectrum sensing, spectrum characterization, coexistence, transmitter detection.**

I. Introduction

The current exclusive allocation and assignment of spectrum to specific technologies and operators has resulted in the over-saturation of popular frequency bands, such as cellular, while other bands, like UHF TV, remain underutilized. As a result, shared spectrum access has become a foundational design principle to address the issues of high costs, decreasing network performance and deteriorated user experience.

A critical requirement of next generation spectrum sharing is detailed characterization of spectrum use. Recent work has resulted in a multitude of spectrum analytics algorithms with various target outcomes including (i) detection of idle or occupied frequency bands [1]–[4], (ii) detection of a particular transmitter type [5], [6], (iii) identification of the number of transmitters present [7], (iv) detection of transmitters' time and frequency activity [7], [8], (v) modulation recognition [9]–[11], (vi) localization [12], and fingerprinting of individual devices [13]. In this paper, we focus on transmitter detection and characterization. Transmitter detection determines the number of transmitters present in a spectrum trace. Transmitter characterization is the identification of all time-frequency blocks occupied by each of the detected transmitters. Transmitter detection and characterization are cornerstones in spectrum-sharing, as they underpin detailed situational awareness necessary for resource allocation and spectrum adjudication. Co-existing technologies can use detection and characterization to inform primary-secondary user interactions and underpin secondary-secondary sharing. Enforcers can use detection and characterization to pinpoint unauthorized spectrum activity. Finally, policy makers can use these capabilities to evaluate the adoption of spectrum regulations and inform new policy based on historic analysis of spectrum use.

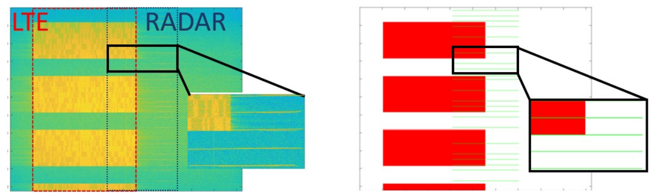

Figure 1. Overlapping LTE and RADAR transmissions in a high-noise setting. Left is a visualization of the raw signal with a zoom in on an area of overlap. Right shows SCAN's detection of the two transmitters (LTE in red and the RADAR in green). This case presents a particularly challenging realistic scenario and demonstrates SCAN's practical applicability.

A particularly challenging and increasingly targeted practical scenario is the detection of narrow-band fleeting signals, such as radar, in the presence of other broadband activity. One such example is presented in Fig. 1 (left), which shows coexisting LTE and navy radar Type 1 [14] in the Citizens Broadband Radio Service (CBRS) bands. The radar activity is short-lived, close to the noise floor and overlaps in time and frequency with the LTE signal. While radars incur minimal spectrum activity and provide ample resource to share, their rapid and accurate detection is critical, as services such as weather forecasting or the national defense rely on radars.

Existing spectrum analytics focus on detecting idle and occupied bands [1]–[3], but do not support per-transmitter characterization of temporal and frequency usage patterns. While some recent work has explored the use of wavelet decomposition [8], or Rayleigh-Gaussian mixture models [7] for transmitter characterization, these methods are either limited to single-transmitter scenarios [8] or struggle with realistic settings involving multiple transmitters with similar signal-to-noise ratio (SNR), or frequency overlap, such as the ones from Fig. 1. Recent work has also employed supervised deep learning [6], [15] to discern specific technologies such as radar or LTE, however, these methods are only applicable to CBRS and do not support characterization of time-frequency activity.

To address these challenges we propose SCAN, a general framework for unsupervised transmitter detection and char-

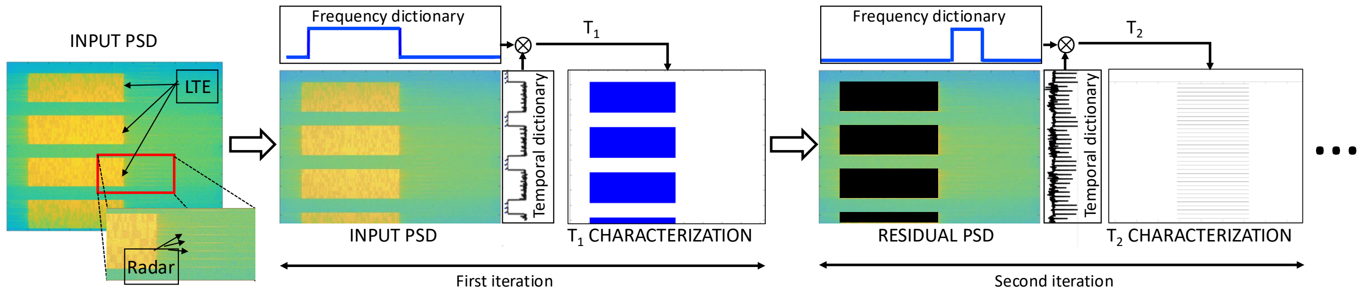

Figure 2. Overview of SCAN's detection process for a sample PSD input with overlapping LTE and radar: The framework learns a sparse dictionary encoding for the transmitter's time and frequency activity. The outer product of these encoding give the full transmitter characterization. It computes a residual PSD matrix, excluding detected regions. This process repeats using the residual as input until the termination criteria are met (described in § V).

acterization based on multi-dictionary sparse representations. SCAN detects all time-frequency blocks of transmitter activity, as illustrated in Fig. 1(right) even in the presence of co-occurring, overlapping, narrow-band/fleeting transmitters, and in diverse interference scenarios. Specifically, we model transmitter detection as a low-rank sparse coding in power spectrum density (PSD) scans, where individual components (rank-1 encodings) map to individual transmitters. Existing multi-dictionary coding solvers are constrained to the same optimizer for all dimensions of the data, e.g. greedy in 2D-Orthogonal Matching Pursuit (OMP) [16] and convex relaxation in Temporal Graph Signal Decomposition (TGSD) [17], [18] and cannot explicitly model domain constraints. Our solution exploits transmitter properties such as occupation of contiguous frequency bands and intermittent temporal activity. We design domain-informed dictionaries and employ them in a novel joint optimization scheme.

Fig. 2 illustrates a detection of radar and LTE using SCAN. SCAN inputs a 2D PSD matrix, where the rows and columns present temporal and frequency activity, respectively. SCAN is iterative and detects one transmitter at a time. In the first iteration, SCAN takes as input the PSD matrix. It then learns the best dictionary representations for a transmitter's frequency and time activity and outputs a detailed transmitter characterization using these learned dictionaries. SCAN then masks out all regions detected as occupied by the first transmitter and supplies the residual PSD as an input to the second step. This process repeats until the stopping criteria is met, at which point all transmitters have been detected and characterized.

We evaluated SCAN with synthetic and real-world traces. Our synthetic traces provide control of the number of transmitters, their time-frequency overlap, and power levels. The realistic traces encompass practical scenarios such as LTE-radar coexistence in CBRS, LoRa, WiFi, ZigBee and LTE traces. We compare SCAN with baselines and show robust and consistent performance, including in very challenging conditions with low-SNR, narrow-band and short-lived transmitters.

This paper makes the following contributions:

• **Novelty:** We propose a general unsupervised method, called SCAN, for transmitter detection and characterization based on multi-dictionary sparse coding. It detects narrow-band, low-power and fleeting transmissions across various coexistence scenarios.

• **Performance:** We evaluate SCAN on (i) synthetic, (ii) controlled over-the-air, and (iii) real-world spectrum scans and demonstrate its superiority over counterparts from the literature in single- and multi-transmitter scenarios.

• **Applicability:** SCAN is unsupervised, and thus, applicable across any spectrum band and technology. We demonstrate this with coexisting radar-LTE in the CBRS bands, and with in-situ detection of LoRa, WiFi, ZigBee and LTE.

II. Related Work

Spectrum characterization has been targeted in the past to a various level of detail and through a variety of methodological approaches. In early cognitive radio of key interest was the detection of idle and occupied spectrum bands [19], however, attributing activity to transmitters was not tackled. Methods using edge detection in raw [1]–[3] or pre-processed [4] PSD scans were predominantly used for this purpose. More recently, a need for transmitter detection and detailed time-frequency characterization has emerged and is tackled through both supervised and non-supervised approaches. In what follows, we detail advances and limitations of recent work.

Energy-based occupancy detection is a widely used group of techniques for spectrum sensing [1]–[4]. In this method, collected PSD values are compared against a predefined threshold. PSD bins that exceed the threshold, are identified as a occupied, whereas those falling below the threshold are deemed idle. Energy detection methods generally have low computational complexity and do not require prior knowledge of spectrum activities. However, choosing an appropriate threshold for energy detectors is often difficult especially in low SNR and dynamically-changing conditions [20]–[24]. This leads to missed detection and false alarms, making edge detection unreliable in realistic noisy and dynamic environments. Furthermore, while these works focus on idle/occupied band detection, they cannot attribute activity to longitudinal transmitter operation, and thus cannot support fine-grained time-frequency transmitter characterization. In contrast, SCAN detects individual time-frequency transmitter activity blocks, and is sensitive in low-SNR regimes.

Detailed transmitter detection and characterization has been tackled through both supervised [6], [15], [25]–[27] and unsupervised [7], [8] methods. AirVIEW [8] uses wavelet-based signal processing and denoising to characterize individual transmitters in high-noise regimes. However, AirVIEW cannot be readily extended to multi-transmitter scenarios. TxMiner [7] uses unsupervised clustering of PSD data for multi-transmitter detection and characterization. However, it falls short in discerning transmitters with similar power levels and cannot model narrow-band and short-lived transmitters that incur minimal spectrum activity. In contrast, SCAN is designed to detect multiple transmitters across various SNR regimes and with narrow-band and short-lived activity.

A counterpart stream of work uses supervised methods for transmitter classification (i.e. detection of the transmitter type). These often rely on deep learning (DL) and treat transmitter detection as an object detection problem [6], [15], [25], [26], [28]. Their purpose is to identify whether a specific transmitter type is present, and not to discern the transmitter's time-frequency activity. In addition, these methods operate in single-transmitter scenarios and are trained to recognize naval radar, WiFi, or LTE signals. Most recently Spectrum Stitching [27] (which we henceforth refer to as STS) proposed a multiclass DL-based semantic spectrum segmentation framework that can detect, characterize, and classify transmitters in both time and frequency at the I/Q level. These methods require extensive training and are not easily applicable for detecting arbitrary transmitter types. Additionally, they fall short in low SNR regimes, as shown in our evaluation. In contrast, SCAN targets detection and characterization (but not classification) for multiple arbitrary transmitter types and across various SNR regimes. SCAN can be complementary to deep-learning based approaches as it can serve as a pre-processing step to enhance low-SNR images before feeding them into a DL framework for transmitter type classification.

III. Background

In this section, we review the evolution of transmitter detection in the literature, and motivate the need for SCAN through several experimental demonstrations.

Transmitter detection is a concept that has evolved to refer to a gradient of spectrum analytics tasks with increasing details of transmitter characterization including active/idle band detection to ascertain the presence of an incumbent [4], [29], [30], transmitter bandwidth detection [6], [25], and more recently detailed characterization of the time-frequency activity of all present transmitters [7], [8], [27]. In this paper we focus on the last task which encompasses and generalizes the previous two. Formally, transmitter characterization algorithms must support the detection of five metrics as depicted in Fig. 3(left), including: (i) the exact number of transmitters present, (ii) the frequency band occupied by each transmitter (Δf), (iii) the active time duration of each transmission (Δt), (iv) the inter-arrival time (Δi), and (v) the gap between consecutive transmissions (ΔT). These five properties comprise a thorough characterization of a transmitter's time-frequency activity.

We demonstrate limitations in existing literature through two toy examples with multiple transmitters sharing the spectrum. The first scenario is based on a controlled over-the-air spectrum trace captured via a USRP B210 sensor (Fig.3), while the second is based on a synthetically generated trace capturing a wide-band long-lived transmitter coexisting with a narrow-band short-lived one (Fig. 4). The over-the-air spectrum scan consists of two intermittent periodic transmitters T_1 and T_2, operating in an unused TV White Spaces channel at center frequencies of 571.9 MHz and 572.1 MHz, respectively, with 3 transmissions each. The gain of the two transmitters is 55 dB resulting in similar sensed power. The transmitters differ in packet size, where T_2's packet size is twice that of T_1. The synthetic trace consists of a narrow-band short-lived transmitter overlapping in frequency with a wide-band transmitter. The wide-band transmitter occupies 100 frequency bins and 30 time steps, and has a mean power level of -85 dBm. The narrow-band transmitter occupies 20 bins and 4 time steps, and has a mean power of -95 dBm.

Fig. 3(right) and Fig. 4(right) illustrate characterization of the above scenarios using TxMiner. Highlighted in red are regions from the trace detected by TxMiner as a transmitter. We first focus on the over-the-air trace characterization in Fig. 3. All spectrum activity is detected as a single transmitter, due to the comparable power level of both transmitters. Furthermore, the temporal behaviour of the second transmitter is not correctly characterized, leaving half of the transmitter activity undetected. The synthetic trace characterization in Fig. 4(right) suffers a different set of problems. TxMiner is only able to detect the wide band transmitter (in red) but fails to detect the frequency occupancy or the temporal behavior of the narrow band transmitter. This is due to the minimal amount of activity generated by the narrow-band transmitter, which makes it challenging for existing work to model and detect the corresponding transmitter. These shortcomings can hinder spectrum sharing, causing missed opportunities or interference with primary users. A fast, sensitive detector like SCAN enables efficient band utilization for opportunistic access.

IV. Preliminaries

PSD data, while extremely noisy, can be sparsely represented via an appropriate basis (dictionary), since transmitter activity (the underlying signal) spans contiguous time-frequency regions. Our proposed method, SCAN, is motivated by sparse dictionary coding [31], hence, we first introduce necessary notation and preliminaries from the literature before describing the method in the following section. The input data for our problem of transmitter detection is a PSD scan $X \in \mathbb{R}^{t\times f}$ with t rows corresponding to time steps and f columns corresponding to frequency bins. A single transmission burst B_j is a contiguously-occupied time-frequency block of constant power, i.e. B_j is a submatrix of X (for example, there are 4 LTE transmissions in Fig. 1). A transmitter $T_i = (B_{ij})$ is a sequence of at least one intermittent transmissions. We model the observed spectrum scan X as a mixture of $b \geq 0$ transmitters and noise:

$$X = \sum_{i=1}^{b} T_i + \epsilon \tag{1}$$

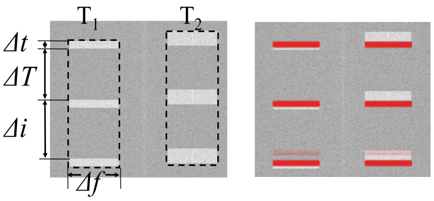

Figure 3. Detection produced by TxMiner [7] in red (right) for a spectrum trace with two non-overlapping transmitters with similar power levels (left). TxMiner fails to separate the two transmitters or correctly characterize their temporal activity.

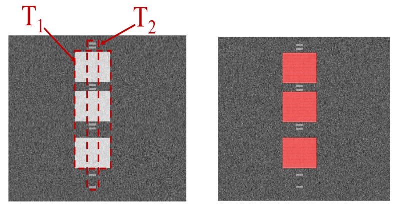

Figure 4. Detection by TxMiner [7] in red (right) for two overlapping transmitters — a narrow-band short-lived and a wideband long-lived; with different power levels (left). TxMiner is unable to detect the short-lived signal.

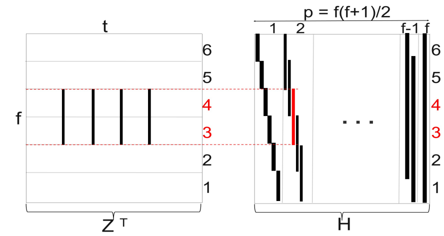

Figure 5. SCAN frequency band selection. (left) Input signal Z^T occupying bins 3-4, (right) a dictionary H with atoms (vertical bars) representing candidate occupied bands, with lengths 1 to f bins. The red atom is best-aligned with the input.

where $\epsilon \in \mathbb{R}^{t \times f}$ represents independently and identically distributed (i.i.d.) Gaussian noise across all elements of the matrix. The noise matrix ϵ has the same dimensions as X. Given X, our goal is to detect all transmitters T_i, i.e. the "location" of frequency-time blocks for each T_i.

The above observation model and associated detection problem aligns closely with the extensive literature on sparse dictionary coding [31]. In its simplest form, a vector signal $x \approx \Phi w$ is approximated as a sparse linear combination of a few atoms from a predefined dictionary Φ, via the coefficients in w. The choice of Φ is critical for performance in downstream tasks [32], [33]. Given the multi-modal nature of spectrum scans X (occupied frequency versus time), a single dictionary is insufficient to characterize both the temporal patterns and frequency bands of a transmission T_i. Instead, for such 2D signals, one can use a separate dictionary for each mode (i.e., multi-dictionary sparse encoding) [17], [34], [35]. The two-dictionary formulation extends the basic one with separate dictionaries for each signal dimension, given as:

$$\min_{Z} f(Z) \quad \text{s.t.} \quad X = \Phi Z H^T, \tag{2}$$

where the left dictionary Φ contains atoms corresponding to column (temporal) patterns, the right dictionary H contains atoms corresponding to row (frequency band) patterns, and Z is a sparse encoding matrix. Here, Z_{ij} represents the sparse coding coefficient for the outer product of the i-th atom in Φ and j-th atom in H ($\Phi_i^T H_j$). The function $f()$ promotes sparsity for Z. Existing solvers for 2D sparse coding adopt either greedy approaches [16] or convex relaxation [34], including imposing low-rank on the encoding matrix Z [17].

V. Problem and Methodology

A. Problem Formulation

Adopting existing signal reconstruction solvers for Eq. (2) to perform transmitter detection according to the model in 1 would i) require non-trivial post-processing (thresholding to convert the reconstruction model into detected transmitters) and ii) ignore prior knowledge about the "shape" of transmitters consisting of intermittent bursts in the same contiguous frequency band. Instead, we "extract" transmitters in X one at a time while representing the signal in each transmitter via a rank-1 multi-dictionary encoding. We also design appropriate analytical dictionaries to represent sequences of contiguous bursts. Mathematically, we model a transmitter T_i as an outer product of left and right dictionary encoding vectors:

$$T_i \approx (\Phi w_i)(H s_i)^T, \tag{3}$$

where s_i is a sparse encoding vector that selects the transmitter's occupied frequency band via a dictionary H and w_i is an analogous vector defining its temporal pattern as a linear combination of atoms in Φ. Additionally, enforcing sparsity for both w_i and s_i would ensure "simple" frequency occupancy and temporal behavior. This sparse coding model for a single transmitter naturally extends to multiple transmitters as:

$$X = \sum_{i=1}^{b} T_i + \epsilon \approx \sum_{i=1}^{b} \Phi w_i (H s_i)^T + \epsilon \tag{4}$$

In other words, the spectrum scan be modeled as a sum of sparse multi-dictionary encodings. Following this, SCAN relies on two key components to identify transmitters: Hs_i identifies a single frequency band of a transmitter's operation and Φw_i models the time-steps where the associated transmissions occur. We require that learned coefficient atom pairs directly map to transmitter locations and their power. Thus, we design custom dictionaries and corresponding solvers for the frequency and temporal modes. We start with the design of a frequency band dictionary H. We note that since a (non-frequency hopping) transmitter occupies a contiguous spectrum band, we can express its bandwidth of operation via a single atom in H, as long as $H \in \mathbb{R}^{f \times p}$ is a dictionary of all possible $p = \frac{f(f+1)}{2}$ frequency sub-bands that span the observation scan X as shown in Fig. 5 (right). In other words, each atom (column) of H is a binary vector with 1s in the frequency bins of the corresponding band. Given that each atom maps to single possible transmission band, a transmitter's encoding vector s_i needs to select a single atom: $||s_i||_0 = 1$.

Having determined the frequency band of a transmitter T_i we next learn its temporal activity (i.e. the temporal intervals of the transmissions B_{ij}). The temporal activity can similarly be expressed as a sparse encoding Φw_i via an appropriate temporal dictionary Φ through a sparse vector of coefficients w_i. The temporal domain of a transmission does not have the clear structure found in the frequency domain and can vary widely across transmitter types. Therefore, it is not feasible to construct a Φ in a similar manner as H. However, we do expect transmissions to follow some high-level patterns such as on/off or potentially periodic behavior. Thus, we can employ appropriate analytical dictionaries such as wavelets, Ramanujan periodic filter banks [36] and others. To encourage sparsity in w_i we adopt a widely used L_1 regularization.

Our **overall formulation of transmitter detection** as an optimization problem is as follows:

$$\min_{w,s} ||X - \sum_{i=1}^{b} \Phi w_i s_i^T H^T||_F^2 + \lambda \sum_{i=1}^{b} ||w_i||_1$$
$$\text{s.t.} \quad ||s_i||_0 = 1, \quad 1 \leq i \leq b$$

where λ is a regularization parameter controlling the sparsity of temporal transmitter encodings w_i.

B. Optimization approach for SCAN

Our formalization of transmitter detection is an instance of a 2-dictionary sparse coding problem: given the fixed dictionaries Φ and H the goal is to estimate all transmitters' coding vectors (w_i, s_i). Existing greedy [16] (2D-OMP) and convex relaxation [17] (TGSD) solutions are not appropriate for our specific formulation as they cannot incorporate domain constraints. 2D-OMP generalizes traditional (1D) OMP by computing 2D (outer-product) atoms from all possible pairs of left and right dictionary atoms, while TGSD employs Alternating Direction Method of Multipliers (ADMM) to solve an L1-regularized objective for both modes. Neither solver is capable of ensuring the critical constraint of transmitters occupying contiguous frequency bands (i.e., the requirement of using only a single atom of H), without which the learned coefficients cannot be directly mapped to transmitters. Moreover, both 2D-OMP and TGSD cannot scale to an exhaustive dictionary such as H, as it will produce a cubic number ($O(tf^2)$) of 2D atoms in 2D-OMP and would require the inversion of a large over-complete dictionary in the case of TGSD.

Thus, instead of enforcing a single approach — greedy OMP or convex relaxation — for both the frequency and the temporal dimension, we use a separate detector for each, catering to the unique properties of transmitters' time and frequency behaviors. Specifically, we detect one transmitter at a time starting with those of highest power. For each transmitter we detect its bandwidth using greedy atom selection and then represent its temporal behavior using a convex relaxation for the aggregate time series within the selected band.

SCAN is presented in Algorithm 1. At a high level SCAN's transmitter detection consists of four steps which are repeated for each transmitter: (1) row-wise mask-aware centering (Steps 5-7) to ensure robustness to varying noise and signal power levels; (2) greedy frequency band selection (Steps 8-10); (3) temporal transmitter activity detection (Steps 11-14); and (4) bookkeeping (Steps 15-21), which checks if a stopping criteria is met, and if not, adds the most recent detection T_i to the list of detected transmitters, and updates the "do-not-detect" mask Ω. Ω is used in subsequent iterations to prevent repeated detection of the same transmitter. Our stopping criteria is adaptive and uses statistical properties of the scan. Specifically, if a detection T_i has power density similar to the average of

Algorithm 1 SCAN

Require: Input $X \in \mathbb{R}^{t \times f}$, quantile threshold q, temporal dictionary Φ
Ensure: A set of transmitters T
1: Initialize mask Ω as all-ones of the same size as X
2: All possible frequency bands $H \in \mathbb{R}^{f \times p}$
3: $\mathbf{n} \in \mathbb{R}^p$ is a vector of atom lengths
4: **for** i=1 to b **do**
5: *// (1) Masked row-wise centering*
6: $\mu_{\mathbf{X}} = [(X \odot \Omega)\mathbf{1}] \oslash (\Omega\mathbf{1})$
7: $Z = (X - \mu_{\mathbf{X}}\mathbf{1}) \odot \Omega$
8: *// (2) Greedy alignment-based frequency selection*
9: $s =$ max-index$(\mathbf{1}ZH \oslash \mathbf{n})$
10: $h_s = H(:, s)$
11: *// (3) Temporal transmitter activity detection*
12: $y = Zh_s$
13: w is the solution for: $\arg\min_w ||y - \Phi w||_2 + \lambda||w||_1$
14: Let g be a 0-1 vector with 1s corresponding to the highest component of $GMM(\Phi w, 2)$
15: *// (4) Book-keeping and check stopping criterion*
16: Compute 0-1 mask transmitter locations $T_i = gh_s^T$
17: **if** $\overline{X(T_i)}$ not in top q-quantile of random transmission windows in X **then**
18: Break
19: **end if**
20: Update detection mask $\Omega = max(\Omega - T_i, 0)$
21: $T = T \cup T_i$
22: **end for**

randomly sampled rectangles in the original scan X (i.e., likely similar power to background noise), it is not added to the set of transmitters and the detection process stops. Next we detail the individual steps of Algorithm 1.

SCAN takes as an input a spectrum trace X, a temporal dictionary Φ and a quantile threshold q used in the stopping condition (described in more details later), and produces a set of transmitter locations $T = \{T_i\}$ as binary matrix with 1s denoting the time-frequency bins occupied by individual transmitters. Before the main detection loop we perform necessary initialization (Steps 1-3). In Step 1 we initialize a detection mask Ω of the same size as X to all 1s. This mask will be updated after each transmitter detection by placing 0s in time-frequency bins occupied by detected transmitters (Step 20). In practice this allows us to disregard regions already allocated to transmitters. In Step 2 we generate the exhaustive frequency dictionary H, where atoms are contiguous runs of 1 for the corresponding frequency band and a value of 0s elsewhere (see Fig.5). Because of this clear mapping between atoms and frequency location, H allows for explicit frequency band detection. In Step 3 we store the atom "lengths" for all atoms in H in a size-p vector $\mathbf{n}$. This vector will help us normalize the alignment scores (described next) so that frequency bands of different width are treated equally.

Steps 4-22 extract one transmitter per loop iteration until all transmitters are detected per the stopping condition. In the centering phase, we compute the row-wise mean μ_X for the data X by excluding masked time-frequency bins marked as 0 in Ω (Step 6). Here $\odot$ denotes element-wise multiplication, while $\oslash$ denotes element-wise division. Intuitively, the μ_X column vector of size t holds the empirical mean power of each row X_t of the input, excluding time-frequency bins marked as 0 in the mask Ω. Next, each row (or time slice) is centered in Step 7, while retaining detected transmissions at 0 based on the mask Ω. We perform the masked row-wise centering of the data in Steps 5-7 to boost transmissions in time steps in which they occur and retain near 0 value in time points without transmissions akin to masked regions.

In Steps 8-10 we greedily select the atom in H with the largest alignment to all time steps of the centered data in an OMP-like fashion. Specifically, in Step 9 we compute H's atom alignments with centered rows as inner products ZH and then aggregate the alignments per atom $\mathbf{1}ZH$. Aggregated atom alignments are normalized by the length of the atoms via an element-wise division by vector $\mathbf{n}$ to avoid giving advantage to atoms corresponding to wider bands. The produced index $s \in [1, p]$ is that of the atom of best average alignment h_s. A visual representation of this selection process is shown in Fig. 5, where the transmitter band in Z^T spans bins $3-4$ corresponding best-aligned atom is marked in red in H. Step 10 stores the column with index s in h_s.

Steps 11-14 identify the temporal (on/off) activity g of the transmitter within the selected band h_s. We first aggregate the centered power density within the detected frequency band h_s to form an activity time series $\mathbf{y}$ in Step 12. Next, we obtain a sparse coding $\mathbf{w}$ of the temporal activity via the atoms in the temporal dictionary Φ (Step 13). This problem is a classical convex relaxation for sparse coding and produces a denoised and smoothed representation Φw. This representation of the temporal activity is biased by the shape of the dictionary Φ. In our experiments, we use Haar wavelets, which with their rectangular shape are well-suited to approximate on/off activity. Finally, the smoothed representation Φw is partitioned using a Gaussian Mixture Model (GMM) and the largest magnitude component (strongest transmitter) is extracted as a 0/1 vector g in Step 14. The GMM separation step is critical as multiple transmitters of varying power levels may reside in the same band and our goal is to extract the one of highest power first and leave the remaining for subsequent iterations.

The frequency $\mathbf{h}_s$ and temporal $\mathbf{g}$ activity vectors are multiplied (outer product) to produce a mask for the detection T_i in step 18. In Steps 17-19 we check if the current detection T_i is noise (according to the stopping criterion described next) and if so, the main detection loop is terminated. If T_i is determined as a transmitter, the detection mask Ω is updated in Step 20 to exclude it by subtracting T_i element-wise and ensuring non-negative values using a max operation. In Step 21, T_i is added to the result set T. This process continues iteratively until the stopping criterion is satisfied.

Stopping criterion. In Steps 17-19 we make a decision of whether to stop detecting more transmitters based on the average power of frequency-time bins in the current detection $\overline{X(T_i)}$. Intuitively, if the average power in the current "strongest" signal component T_i is similar to that of background noise, we must have detected all transmitters in previous iterations. The challenge is that we do not have a reliable statistical characterization of the background noise for an arbitrary input scan X. Thus, we estimate a scan's background noise via random sampling. Specifically, we estimate a background noise distribution once in the initialization phase (steps not shown for simplicity) for randomly sampled rectangular windows of fixed size (5×5 bins). Using the sampled data, we form a noise distribution. If the average power of a transmitter detection $\overline{X(T_i)}$ falls in the top q-quantile of the noise distribution, the detection is considered a transmitter and otherwise it is considered noise. In our experiments we use $q = 5$ which resulted in reliable and accurate detection and terminations at the correct number of transmitters for all experimental traces.

Algorithmic complexity. The complexity of each iteration in SCAN is dominated by the projection of the compressed signal $(\mathbf{1}Z) \in \mathbb{R}^{1 \times f}$ on the over-complete basis $H \in \mathbb{R}^{f \times p}$. Because the number of atoms $p = f(f+1)/2$ in H is $O(f^2)$, the overall complexity of the matrix multiplication is $O(f^3)$. This has to be preformed once for each transmitter detection resulting in a total complexity $O(bf^3)$. Note, however, that there are opportunities to speed up the execution by i) sub-sampling the data X in time and/or frequency, by ii) pre-selecting atoms in H based on their alignment to the average time slice and iii) by employing domain knowledge about target transmitter properties (e.g. allowable bandwidth). Data sub-selection is effective for high resolution over-the-air scans. For example, if the shortest lasting transmission is sampled at high temporal resolution consisting of at least m time steps, we can drop every $m-1$ time steps and still detect the transmitter effectively. Since we only select top aligned atoms of H we can also work with a reduced size H by pre-selecting atoms of high alignment with the average row in the data X.

VI. Evaluation

We now showcase SCAN across various transmitter co-occurrence scenarios, noise regimes and with realistic data, and in comparison with counterparts from the literature.

A. Experimental setup

Data. We evaluate SCAN on synthetic data and controlled over-the-air traces. Our synthetic dataset, generated as a 2D matrix of PSD values from N + 1 normal distributions $G_i(x|\mu_i, \sigma_i)$, allows us to control the SNR, variance, and co-occurrence of transmitters where $i \in (1, N)$ is the number of transmitters we are looking to generate. The G_{N+1}-th distribution generates noise with a mean and standard deviation of -109 dBm and 3.94, based on empirical measurements from a USRP B210-based spectrum sensor. The transmitter distributions are detailed in individual experiments.

For our controlled over-the-air traces, we use two types of traces: (i) some from a testbed we built with two transmitters and a sensor, and (ii) some from two recent papers [14],

[27], which comprise over-the-air traces of WiFi, ZigBee, Bluetooth, LoRa, LTE and CBRS Radar-LTE . For our testbed, the transmitters are USRP B210 radios with LP0410 Log Periodic PCB directional antennas, connected to laptops with Intel i7-5600 CPU. The sensor is a RTL-SDR with a wide-band multi-polarized antenna, connected to a PC with an Intel i7-4770 CPU. All hosts run Ubuntu 16 with GNURadio 3.7. Both transmitters and the sensor are realized with GNURadio scripts. The collected traces are IQ samples converted to PSD for analysis. Further detail about the transmitters and sensor configurations is provided in § VI-C1. To determine the ground truth binary matrix G for each transmitter, we compute the time/frequency activity blocks as follows: $\Delta f = \frac{B_w \times fft}{f_s}$, $\Delta t = \frac{T_{burst} \times f_s}{fft}$, $\Delta T = \frac{T_{sleep} \times f_s}{fft}$, $\Delta i = \Delta t + \Delta T$. Where B_w is the bandwidth in Hz, f_s is the sampling rate, T_{burst} is the burst duration, T_{sleep} is the sleep time between transmissions.

Baselines. We compare SCAN with three baselines: AirVIEW [8], TxMiner [7] and STS [27] selecting the most suitable method(s) based on the dataset. AirVIEW is applied to synthetic traces with a single transmitter, as it is specifically designed for single-transmitter characterization in low-SNR scenarios. TxMiner is used for both single and multiple transmitter traces as it can detect and characterize multiple transmitters. STS requires IQ input, so we apply it to over-the-air traces, since synthetic traces consist of PSD values.

Metrics. We aim to identify all time-frequency regions a transmitter occupies. Thus, we measure SCAN's accuracy using the Jaccard similarity (J) between ground truth (G) and detection (T_i), where $J = \frac{|T_i \cap G|}{|T_i \cup G|}$. This 2D Jaccard similarity inherently includes TPR and FPR, thus providing a better performance metric with respect to ground truth. Results are averaged over 100 realizations.

B. SCAN with controlled synthetic data

We begin our evaluation on synthetic data with tight control on transmitter count, properties, and co-occurrence scenarios. We use TxMiner and AirVIEW as baselines.

*1) **Effects of signal strength and variance**:* Our first goal is to evaluate SCAN's performance in low-SNR/high-noise regimes compared to baselines. We use traces of a single transmitter with increasing signal power and variance. The generated transmitter occupies 120 frequency bins and 10 time steps per burst. Fig. 6(left) shows that SCAN's accuracy remains nearly perfect and outperforms baselines across all regimes, even at -106 dBm transmitter power with SNR only 3 dB above the noise floor. In contrast, AirVIEW and TxMiner deteriorate at low signal power. Fig. 6(middle) shows SCAN's accuracy as the signal variance increases. The traces contain a single transmitter with a mean power of -102 dBm. SCAN performs near optimally until the variance reaches 20, then slightly decreases. TxMiner consistently scores around 0.7, as it confuses the transmitter and noise. AirVIEW's performance substantially declines with increasing signal variance.

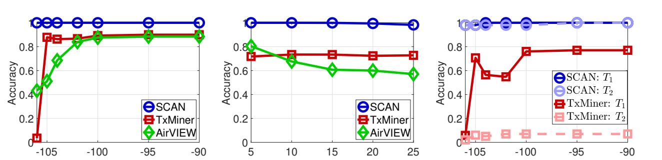

Figure 6. Effects of signal strength and variance on performance. Accuracy vs. mean signal power (left), Accuracy vs. signal power variance (middle), and Accuracy vs mean signal power (right) for a two transmitter scenario.

Next, we evaluate SCAN's performance with two non-overlapping, equi-power transmitters in low-SNR/high-noise regimes, and compare it to TxMiner only, as AirVIEW is not designed for multi-transmitter detection. The first transmitter (T_1) occupies 120 frequency bins and 10 time steps per burst, while the second transmitter (T_2) occupies 100 frequency bins and 5 time steps per burst. Fig. 6(right) shows that SCAN accurately detects and separates each transmitter even at low signal power. In contrast, TxMiner combines the transmissions due to their equal signal power into a single transmitter, resulting in nearly zero accuracy for T_2.

*2) **Performance with wide- and narrowband signals**:* The detection of shortlived and narrowband transmitters, akin radar pulses, is extremely challenging, especially in the face of wideband interference [37]. Simultaneously, the reliable detection of such signals is increasingly critical for emerging spectrum-sharing applications [38]. Thus, we showcase SCAN's applicability to such scenarios in both synthetic and real-world traces. Here, we evaluate SCAN with two co-occurring transmitters: a strong wideband, long-lived transmitter (LL) and a weak narrowband, short-lived transmitter (SL). We control the transmitters' SNR and time-frequency activity. The LL signal spans 100 frequency bins over 30 time steps, while the SL signal's bandwidth varies from 20% to 100% of the LL signal, and a duration of 2 time steps.

We first evaluate the effects of frequency overlap on the detection accuracy. Fig. 7(left) shows accuracy as a function of the percent overlap between the LL (at -85 dBm) and SL (at -95 dBm). SCAN accurately detects each transmitter, whereas TxMiner fails to separate the SL transmitter from the LL, detecting them as one due to the few samples representing SL. This highlights SCAN's robustness in detecting short-lived, narrow-band transmitters even when they overlap in frequency.

Next, we explore the impact of SNR on LL-SL separation. With a 20% bandwidth overlap, we vary the signal power of each transmitter as shown by the two x-axes of Fig. 7(right). SCAN remains robust even at very low SNRs for both transmitters. TxMiner, however, performs poorly even at high SNRs, deteriorating further as noise increases due to its inability to separate SL transmitters. These results demonstrate SCAN's ability to accurately detect narrow-band, short-lived transmitters in low SNR regimes.

*3) **Performance with varying power difference between transmitters**:* We evaluate the impact of the power differences between co-occurring transmitters on SCAN. We generate two non-overlapping transmitters with the following burst dimensions: T_1 with 120 frequency bins and 10 time steps; and T_2 with 100 bins and 5 time steps. Starting with both transmitters at -80 dBm, we increase T_2's power to -60 dBm.

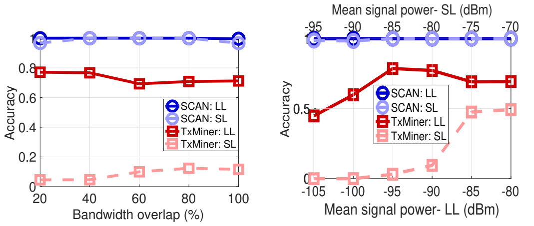

Figure 7. Detection for narrowband and wideband transmitters with increasing bandwidth overlap (left) and increasing signal power (right).

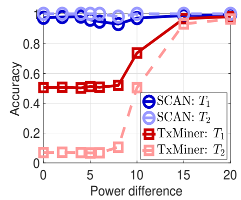

Figure 8. Two transmitters with increasing power difference.

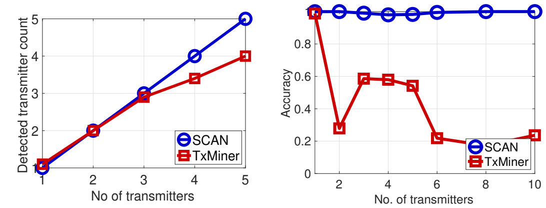

Figure 9. Performance with increasing number of transmitters. SCAN detects the correct number of transmitters (Left) and gives accurate detection for each transmitter activity (Right).

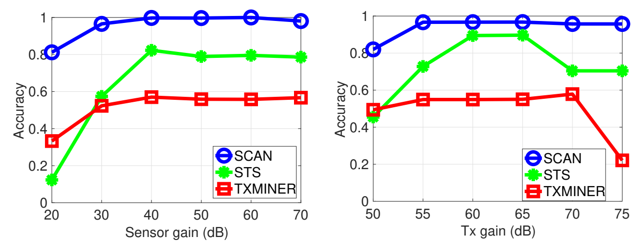

Figure 10. Effect of varying the sensor's gain (left) and transmitters gain (right) for two non-overlapping transmitters.

Fig. 8 shows detection accuracy for each transmitter using SCAN and TxMiner. SCAN maintains high accuracy even when both transmitters have the same power level, whereas TxMiner struggles to distinguish between them with power differences of 10 dBm or less. This demonstrates SCAN's applicability to transmitters with similar power.

*4) **Performance with increasing number of transmitters**:* We evaluate SCAN's performance with an increasing number of transmitters, considering up to 10. Each transmitter has a random temporal pattern, occupies 100 frequency bins, and generates periodic bursts of 10 time steps. Transmitter power levels differ by at least 10 dBm.

First, we explore SCAN and TxMiner's ability to detect the number of transmitters in a trace. Fig. 9(left) shows that as the transmitter count increases from 1 to 5, SCAN accurately detects the expected number, while TxMiner underestimates after 3 transmitters. Next, we examine individual transmitter detection accuracy as the number of transmitters increases, as shown in Fig. 9(right). The y-axis shows average accuracy, calculated as the sum of individual transmitter detection accuracy divided by the expected number of transmitters. SCAN not only detects the correct number of transmitters but does so with high accuracy, significantly outperforming TxMiner.

C. SCAN with over-the-air data

Next, we explore SCAN's applicability to real-world over-the-air data using controlled traces collected in our lab, and data from [27] and [14]. We compare SCAN to STS and TxMiner. STS operates in two steps: first, semantic segmentation to isolate active regions in a scan, and then, classification to assign these regions to one of five known candidates in a supervised manner. Since SCAN is only concerned with segmentation, and not transmitter classification, we only compare with the STS's segmentation, and skip classification.

*1) **Varying sensor/transmitter gain**:* We evaluate SCAN with traces from the setup in § VI-A. T_1 transmits 800 bytes/second at 0.25 MHz bandwidth and 572.1 MHz frequency. T_2 transmits 400 bytes/second at 0.25 MHz bandwidth and 571.9 MHz frequency. The sensor, placed equidistant from the transmitters with line of sight, has 0.5 MHz bandwidth, 6 sec dwell-delay, and 572 MHz center frequency.

First, we evaluate SCAN's performance with transmitters at 65 dBm, while varying the sensor's gain. Fig. 10(left) shows SCAN maintains high accuracy across gains, slightly reducing at 20 dBm where signal power is low, and outperforms baselines. Next, we evaluate SCAN's performance with a fixed sensor gain of 60 dBm, while varying the transmitters' gain. Fig. 10(right) shows SCAN maintains high accuracy across different transmitter gains. STS performs well only at 60 and 65 dBm; its accuracy decreases below 60 dBm due to low signal power and above 65 dBm due to noise and hardware imperfections. TxMiner remains consistently low and deteriorates further at 75 dBm due to high noise.

*2) **Qualitative evaluation with over-the-air traces**:* We next evaluate SCAN on over-the-air signals of four commercial technologies, collected in an uncontrolled RF environment as described in [27]. Due to the lack of ground truth (i.e. a transmitter/noise label for each PSD value), we use qualitative evaluation, showing individual detection in different color. Table I shows that SCAN accurately detects all transmitter types, including LoRa, which is narrowband and frequency-chirping. STS, on the other hand, incurs a large number of false positive detections around the target signals.

*3) **SCAN's applicability in CBRS**:* CBRS [15], a recent shared spectrum technology, allows broadband communications in Navy radar bands when radar is absent. Radar pulses are extremely short-lived, must be detected within 60 seconds [38], [39] to avoid interference with defense applications. This is challenging, especially in low-SNR regimes, as radar pulses are hard to distinguish from surrounding noise.

We showcase SCAN's practical applicability to CBRS and beyond, by exploring an over-the-air trace of LTE and radar [14], shown in Fig. 1 (left). The LTE bandwidth is 15 MHz, while the radar bandwidth is 2 MHz with a pulse width of 0.5 μs and SINR of 19.26 dB. The radar activity significantly overlaps with the LTE transmitter. As shown in Fig. 1 (right), SCAN successfully discerns the two transmitters and characterizes all corresponding activity, including overlapping

Table I
(LEFT) SPECTROGRAM OF REAL-WORLD OVER-THE-AIR DATASET [27] SHOWING LORA, LTE DOWNLINK, WIFI, AND ZIGBEE.(MIDDLE) SCAN'S DETECTION RESULT, WITH EACH DETECTED TRANSMITTER HIGHLIGHTED IN A DISTINCT COLOR. (RIGHT) DETECTION FROM STS [27].

Transmitter Type	Spectrogram	SCAN	STS
LoRa	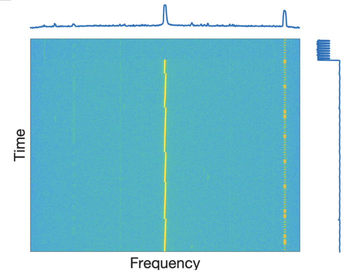	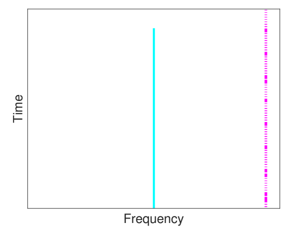	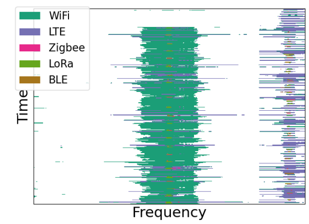
LTE-DL	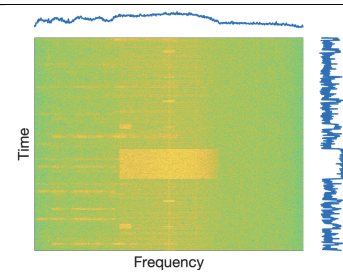	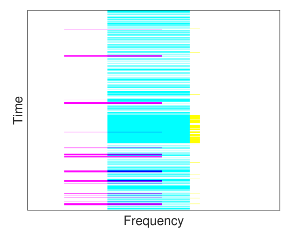	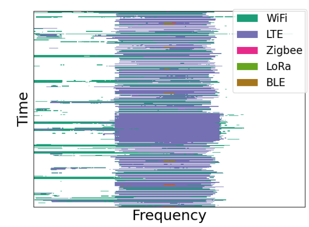
WiFi	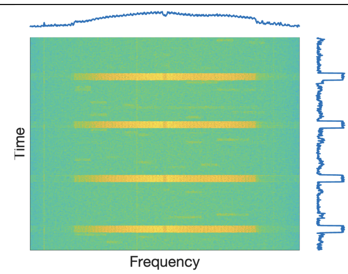	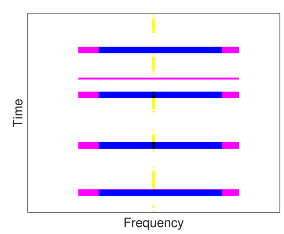	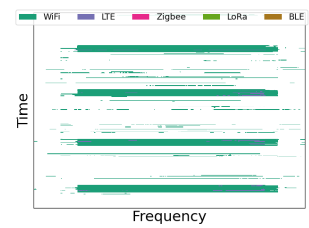
Zigbee	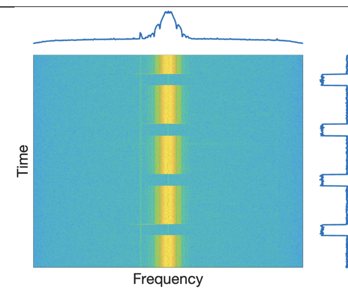	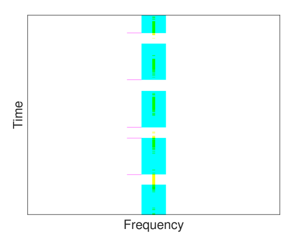	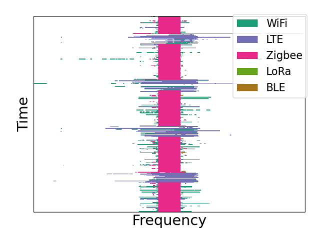

transmissions. SCAN processes this trace in 12 seconds on a personal laptop using MATLAB, meeting the requirements for CBRS users to vacate the spectrum.

VII. DISCUSSION AND CONCLUSION

Spectrum analysis is crucial for opportunistic spectrum access but is challenging with noisy scans, coexisting transmitters with partial time or frequency overlap, and interfering narrow- and wideband transmitters. To address these issues and enable robust, rapid detection of multiple transmitters, we designed SCAN—a framework for unsupervised transmitter detection and characterization. SCAN is an OMP-based algorithm using sparse dictionary encoding to detect transmitters in a spectrum scan and characterize their time-frequency activity.

We evaluate SCAN's performance across various coexistence scenarios in challenging SNR and noise regimes. SCAN successfully detects narrow-band, short-lived, and low-SNR transmitters, even with simultaneous time and frequency overlaps. Further research into SCAN's applicability to mobile and frequency hopping transmitters such as BLE will be necessary, as the H dictionary, is currently designed for transmitters with contiguous frequency bands. Developing a custom H dictionary for mobile transmitters is left for future research. The authors have provided public access to their code at https://doi.org/10.5281/zenodo.14618294

VIII. ACKNOWLEDGMENTS

This work was supported through NSF grants AST-2132700, CNS-1845858 and CMMI-1831547.

REFERENCES

[1] R. Umar, A. U. H. Sheikh, and M. Deriche, "Unveiling the Hidden Assumptions of Energy Detector Based Spectrum Sensing for Cognitive Radios," *IEEE Communications Surveys & Tutorials*, vol. 16, no. 2, pp. 713–728, 2014.

[2] Z. Ye, G. Memik, and J. Grosspietsch, "Energy detection using estimated noise variance for spectrum sensing in cognitive radio networks," in *2008 IEEE Wireless Communications and Networking Conference*, pp. 711–716, IEEE, 2008.

[3] T. Yucek and H. Arslan, "A survey of spectrum sensing algorithms for cognitive radio applications," *IEEE Communications Surveys Tutorials*, vol. 11, pp. 116–130, Jan 2009.

[4] Z. Tian and G. B. Giannakis, "A Wavelet Approach to Wideband Spectrum Sensing for Cognitive Radios," in *2006 1st International Conference on Cognitive Radio Oriented Wireless Networks and Communications*, pp. 1–5, 2006.

[5] S. S. Hong and S. R. Katti, "DOF: A Local Wireless Information Plane," in *Proceedings of the ACM SIGCOMM 2011 Conference*, pp. 230–241, 2011.

[6] S. Sarkar, M. Buddhikot, A. Baset, and S. K. Kasera, "DeepRadar: A deep-learning-based environmental sensing capability sensor design for CBRS," in *Proceedings of the 27th Annual International Conference on Mobile Computing and Networking*, pp. 56–68, 2021.

[7] M. Zheleva, R. Chandra, A. Chowdhery, A. Kapoor, and P. Garnett, "TxMiner: Identifying transmitters in real-world spectrum measurements," in *2015 IEEE International Symposium on Dynamic Spectrum Access Networks (DySPAN)*, pp. 94–105, 2015.

[8] M. Zheleva, P. Bogdanov, T. Larock, and P. Schmitt, "AirVIEW: Unsupervised transmitter detection for next generation spectrum sensing," in *IEEE INFOCOM 2018 - IEEE Conference on Computer Communications*, pp. 1–2, 2018.

[9] W. Xiong, P. Bogdanov, and M. Zheleva, "Robust and efficient modulation recognition based on local sequential IQ features," in *IEEE INFOCOM 2019-IEEE Conference on Computer Communications*, pp. 1612–1620, IEEE, 2019.

[10] H. Gang, L. Jiandong, and L. Donghua, "Study of modulation recognition based on HOCs and SVM," in *2004 IEEE 59th Vehicular Technology Conference. VTC 2004-Spring (IEEE Cat. No. 04CH37514)*, vol. 2, pp. 898–902, IEEE, 2004.

[11] A. K. Nandi and E. E. Azzouz, "Modulation recognition using artificial neural networks," *Signal processing*, vol. 56, no. 2, pp. 165–175, 1997.

[12] J. Shen, A. F. Molisch, and J. Salmi, "Accurate Passive Location Estimation Using ToA Measurements," *IEEE Transactions on Wireless Communications*, vol. 11, pp. 2182–2192, June 2012.

[13] S. S. Hanna and D. Cabric, "Deep learning based transmitter identification using power amplifier nonlinearity," in *2019 International Conference on Computing, Networking and Communications (ICNC)*, pp. 674–680, IEEE, 2019.

[14] C. Tassie, A. Gaber, V. Chaudhary, N. Soltani, M. Belgiovine, M. Loehning, V. Kotzsch, C. Schroeder, and K. R. Chowdhury, "Real-world Radar and LTE Signals Dataset Collected Over-the-air in Shared CBRS Band ," 2022.

[15] N. Soltani, V. Chaudhary, D. Roy, and K. Chowdhury, "Finding waldo in the cbrs band: Signal detection and localization in the 3.5 ghz spectrum," in *GLOBECOM 2022-2022 IEEE Global Communications Conference*, pp. 4570–4575, IEEE, 2022.

[16] Y. Fang, J. Wu, and B. Huang, "2D sparse signal recovery via 2D orthogonal matching pursuit," *Science China Information Sciences*, vol. 55, pp. 889–897, 2012.

[17] M. J. McNeil, L. Zhang, and P. Bogdanov, "Temporal graph signal decomposition," in *Proceedings of the 27th ACM SIGKDD Conference on Knowledge Discovery & Data Mining*, pp. 1191–1201, 2021.

[18] M. McNeil and P. Bogdanov, "Multi-dictionary tensor decomposition," in *2023 IEEE International Conference on Data Mining (ICDM)*, pp. 1217–1222, IEEE, 2023.

[19] A. T. Hoang, Y.-C. Liang, and Y. Zeng, "Adaptive joint scheduling of spectrum sensing and data transmission in cognitive radio networks," *IEEE Transactions on Communications*, vol. 58, no. 1, pp. 235–246, 2010.

[20] X. Ling, B. Wu, H. Wen, P.-H. Ho, Z. Bao, and L. Pan, "Adaptive Threshold Control for Energy Detection Based Spectrum Sensing in Cognitive Radios," *IEEE Wireless Communications Letters*, vol. 1, no. 5, pp. 448–451, 2012.

[21] R. N. Prashob, A. Vinod, and A. K. Krishna, "An adaptive threshold based energy detector for spectrum sensing in cognitive radios at low SNR," in *2010 IEEE International Conference on Communication Systems*, pp. 574–578, IEEE, 2010.

[22] J. Lee, H. Wang, S. Kim, and D. Hong, "Sensing threshold control for fair coexistence of heterogeneous systems in open spectrum," *IEEE transactions on wireless communications*, vol. 8, no. 12, pp. 5773–5778, 2009.

[23] K. Kim, Y. Xin, and S. Rangarajan, "Energy detection based spectrum sensing for cognitive radio: An experimental study," in *2010 IEEE Global Telecommunications Conference GLOBECOM 2010*, pp. 1–5, IEEE, 2010.

[24] A. Ahmed, Y. F. Hu, and J. M. Noras, "Noise variance estimation for spectrum sensing in cognitive radio networks," *AASRI Procedia*, vol. 9, pp. 37–43, 2014.

[25] W. M. Lees, A. Wunderlich, P. J. Jeavons, P. D. Hale, and M. R. Souryal, "Deep Learning Classification of 3.5-GHz Band Spectrograms With Applications to Spectrum Sensing," *IEEE Transactions on Cognitive Communications and Networking*, vol. 5, no. 2, pp. 224–236, 2019.

[26] A. Selim, F. Paisana, J. A. Arokkiam, Y. Zhang, L. Doyle, and L. A. DaSilva, "Spectrum monitoring for radar bands using deep convolutional neural networks," in *GLOBECOM 2017-2017 IEEE Global Communications Conference*, pp. 1–6, IEEE, 2017.

[27] D. Uvaydov, M. Zhang, C. P. Robinson, S. D'Oro, T. Melodia, and F. Restuccia, "Stitching the Spectrum: Semantic Spectrum Segmentation with Wideband Signal Stitching," in *IEEE INFOCOM 2024*, May 2024.

[28] W. Zhang, M. Feng, M. Krunz, and A. Hossein Yazdani Abyaneh, "Signal Detection and Classification in Shared Spectrum: A Deep Learning Approach," in *IEEE INFOCOM*, pp. 1–10, 2021.

[29] L. Yang, W. Hou, L. Cao, B. Y. Zhao, and H. Zheng, "Supporting Demanding Wireless Applications with Frequency-agile Radios.," in *NSDI*, pp. 65–80, 2010.

[30] Y. Yuan, P. Bahl, R. Chandra, P. A. Chou, J. I. Ferrell, T. Moscibroda, S. Narlanka, and Y. Wu, "KNOWS: Cognitive Radio Networks Over White Spaces," in *2007 2nd IEEE International Symposium on New Frontiers in Dynamic Spectrum Access Networks*, pp. 416–427, April 2007.

[31] Z. Zhang, Y. Xu, J. Yang, X. Li, and D. Zhang, "A survey of sparse representation: algorithms and applications," *IEEE access*, vol. 3, pp. 490–530, 2015.

[32] Z. J. Xiang, Y. Wang, and P. J. Ramadge, "Screening tests for lasso problems," *IEEE transactions on pattern analysis and machine intelligence*, vol. 39, no. 5, pp. 1008–1027, 2016.

[33] K. Fujii and T. Soma, "Fast greedy algorithms for dictionary selection with generalized sparsity constraints," *Advances in Neural Information Processing Systems*, vol. 31, 2018.

[34] A. Ghaffari, M. Babaie-Zadeh, and C. Jutten, "Sparse decomposition of two dimensional signals," in *2009 IEEE international conference on acoustics, speech and signal processing*, pp. 3157–3160, IEEE, 2009.

[35] "Low Rank Multi-Dictionary Selection at Scale, author=Ma, Boya and McNeil, Maxwell and Magner, Abram and Bogdanov, Petko," in *Proceedings of the 30th ACM SIGKDD Conference on Knowledge Discovery and Data Mining*, pp. 2106–2117, 2024.

[36] S. V. Tenneti and P. Vaidyanathan, "Nested periodic matrices and dictionaries: New signal representations for period estimation," *IEEE Transactions on Signal Processing*, vol. 63, no. 14, pp. 3736–3750, 2015.

[37] K. Doke, S. Sarkar, B. Okoro, D. Cabric, and M. Zheleva, "RadVIEW: Robust radar detection and characterization in high-noise regimes," in *IEEE DySPAN*, IEEE DySPAN, 2024.

[38] R. Caromi, M. Souryal, and W.-B. Yang, "Detection of incumbent radar in the 3.5 GHz CBRS band," in *2018 IEEE Global Conference on Signal and Information Processing (GlobalSIP)*, pp. 241–245, IEEE, 2018.

[39] A. Sahoo, N. El Ouni, and V. Shenoy, "A study of timing constraints and SAS overload of SAS-CBSD protocol in the CBRS band," in *2019 IEEE Globecom Workshops (GC Wkshps)*, pp. 1–6, IEEE, 2019.